

Electric field induced metallic behavior in thin crystals of ferroelectric α -In₂Se₃

Justin R. Rodriguez^{1,2}, William Murray^{3,2}, Kazunori Fujisawa^{1,2}, Seng Huat Lee^{1,2}, Alexandra L. Kotrick^{1,2}, Yixuan Chen^{1,2}, Nathan Mckee^{1,2}, Sora Lee^{4,2}, Mauricio Terrones^{1,2}, Susan Trolier-McKinstry^{4,2}, Thomas N. Jackson^{3,2}, Zhiqiang Mao^{1,2}, Zhiwen Liu^{3,2}, Ying Liu^{1,2,†}

¹*Department of Physics, Pennsylvania State University, University Park, PA 16802, USA.*

²*Materials Research Institute, Pennsylvania State University, University Park, PA 16802, USA.*

³*Department of Electrical Engineering, Pennsylvania State University, University Park, PA 16802, USA*

⁴*Department of Materials Science and Engineering, Pennsylvania State University, University Park, PA 16802, USA*

†Corresponding author. Email: yxl15@psu.edu

Abstract

Ferroelectric semiconductor field effect transistors (FeSmFETs), which employ ferroelectric semiconducting thin crystals of α -In₂Se₃ as the channel material as opposed to the gate dielectric in conventional ferroelectric FETs (FeFETs) were prepared and measured from room to the liquid-helium temperatures. These FeSmFETs were found to yield evidence for the reorientation of the electrical polarization and an electric field induced metallic state in α -In₂Se₃. Our findings suggest that FeSmFETs can serve as a platform for the fundamental study of ferroelectric metals as well as the exploration of potential applications of semiconducting ferroelectrics.

Ferroelectricity is defined by the formation of spontaneous electrical polarization in a non-centrosymmetric crystal and the reorientation of the polarization between crystallographically defined directions by the application of an external electric field¹. Ferroelectrics have been used to store data in either a capacitor or a ferroelectric field-effect transistor (FeFET)^{2,3} configuration, the latter of which features a ferroelectric gate dielectric and a non-ferroelectric semiconducting channel. FeFETs provide not only fast and non-volatile data storage, but also a pathway towards “logic in memory” functions. However, the commercialization of FeFETs has encountered multiple obstacles ranging from retention time originating from the depolarization field and the gate leakage current⁴ to endurance limited mainly by interface charge traps⁵. A FeFET variation which replaces the semiconducting channel in the conventional FET with a *ferroelectric* semiconducting channel but retains the non-ferroelectric gate dielectric was demonstrated recently⁶. This produces an “on” (or “off”) state without an applied gate voltage, similar to a traditional FeFET. Such a device is referred to as a ferroelectric semiconductor field effect transistor (FeSmFET).

It is interesting to ask whether the “on” state in the FeSmFET can be a metallic state, which will make the transition from the “on” to the “off” state a ferroelectric metal-insulator transition. Anderson and Blount⁷ examined the structural transition found in metallic V₃Si and suggested that the formation of ionic displacements along a polar axis, which led to the loss of inversion symmetry, would be required for the occurrence of the apparent continuous phase transition seen in V₃Si. Furthermore, they suggested that such a state should be called a “ferroelectric metal.” Being a metal appears to be inconsistent with the accepted definition of ferroelectricity as mobile charge carriers in a bulk metal will effectively screen any electric field, making the reorientation of the polarization unlikely. Nevertheless, metals showing the presence of electrical dipoles from ionic displacements along with a well-defined polar axis, such as LiOsO₃^{8,9}, Ca₃Ru₂O₇¹⁰, and other materials¹¹, have attracted much attention in recent years even though the issue of whether the dipoles found in these materials are spontaneously ordered and reversible has not been resolved. Interestingly, the difficulty in reversing the polarization in a metal can be circumvented for a ferroelectric 2D crystal. A vertical electrical field, applied to a 2D crystal of 1T'-WTe₂ by a top and a bottom gate, was shown to lead to sharp jumps in sample conductance, which was attributed to polarization reversal¹². However, direct evidence for ferroelectricity in 2D 1T'-WTe₂ is still lacking.

In_2Se_3 , a layered transition metal chalcogenide (TMC) featuring a van der Waals interlayer coupling and an energy gap of 1.4 eV, was predicted¹³ to be ferroelectric down to 1-unit-cell thickness in both α - and β -phases. Supporting evidence for ferroelectricity in In_2Se_3 was found via piezoelectric force microscopy (PFM)^{14,15,16,17,18} and second harmonic generation (SHG)^{18,19,20}, with a transition temperature up to 700 K¹⁹. Extensive device work carried out in the last few years also supports ferroelectricity in this layered TMC. An on/off state was found in rectifying devices by sweeping the source-drain voltage^{14,15,16,17,21}, revealing distinct hysteresis loops suggesting complex orientations of the polarization^{13,14,16,19}. In the pioneering work of the FeSmFET featuring thin crystals of α - In_2Se_3 and a gate dielectric of 90-nm-thick SiO_2 or 15-nm-thick HfO_2 , respectively, large clockwise and counter-clockwise hysteresis loops were found in gate voltage sweeps⁶. The hysteresis was shown to persist down to 80 mK, making it unlikely that the observed hysteresis at such a low temperature is due to charge traps. These observations strongly support the existence of ferroelectricity in α - In_2Se_3 . However, the most explicit demonstration of ferroelectricity in α - In_2Se_3 was obtained in a stacked capacitor/FET device²². This device consists of monolayer graphene on a SiO_2/Si substrate that functions as a bottom gate. The graphene is also the bottom electrode for a capacitor featuring a two-layer dielectric combining an insulating monolayer or bilayer of hexagonal boron nitride (hBN) and an atomically thin, semiconducting crystal of α - In_2Se_3 , which was covered by a top metal electrode/gate. The electric field applied between the graphene and the top electrode was used to reorient the polarization in α - In_2Se_3 . The graphene sandwiched between SiO_2 and hBN functioned as a charge detector through the position of the charge neutral point (CNP) in sample resistance *vs.* the gate voltage curves. From the clear and systematic shift in CNP as the polarization was flipped, a polarization value of $0.92 \mu\text{C}/\text{cm}^2$ was estimated under an external field of $5 \times 10^5 \text{ V}/\text{cm}$, which is reasonably close to the theoretically predicted¹³ value of $0.6 \mu\text{C}/\text{cm}^2$.

The in- and out-of-plane resistivities of α - In_2Se_3 crystals grown by a modified Bridgman method used in this work, obtained from 4-point probe on bulk crystals using electrical contacts made by Ag paint, showed a variable-range hopping (VRH) conduction at low temperatures (below $\sim 40 \text{ K}$, see Fig. 1a) after the unintentionally doped charge carriers are frozen out. Thin crystals of α - In_2Se_3 were obtained by mechanical exfoliation from a bulk crystal and deposited onto a heavily doped silicon chip with 300-nm thick thermally grown surface of SiO_2 . The thickness of a thin crystal of α - In_2Se_3 was determined by atomic force microscope (AFM) after the transport measurements

were carried out. Two types of FeSmFET featuring a Hall bar (Fig. 1e) and traditional FET (Fig. S1a in Supplementary Materials (SM)) pattern, respectively, were prepared by photolithography with electrodes of 5 nm of Ti and 45 nm of Au. The parameters for the four devices used in the present study are shown in Table S1 in SM. DC Electrical transport measurements were carried out in a Quantum Design Physical Property Measurement System (PPMS) equipped with a 9 T superconducting magnet that features a base temperature of 1.8 K. For temperature varying measurements, the device was cooled/warmed at zero gate voltage unless otherwise specified.

To characterize the thin crystals of α -In₂Se₃, Raman spectroscopy, photoluminescence (PL) and second harmonic generation (SHG) measurements were used. The Raman spectra (Fig. 1b) confirmed that the crystals used were α -In₂Se₃²³. An energy gap value of 1.4 eV was revealed in the PL measurements (Fig. 1c), consistent with that found in the literature²³. Strong SHG signals with the expected six-fold symmetry were also found (Fig. 1d), demonstrating that our α -In₂Se₃ crystal indeed belongs to the $R3m$ space group^{17,18,19}.

Source-drain current *vs.* voltage (I_D *vs.* V_{DS}) characteristics were measured on the FeSmFETs at fixed gate voltages (V_G). The results for Sample A (Fig. 1e) with a channel length of 12 μ m and thickness of 110 nm are shown in Fig. 2 for V_G increasing from -75 to 75 V and back to -75V. No saturation in I_D was observed in this range of the gate voltage up to 10 V for all V_G values. Given that I_D for negative V_G is lower than I_D for the positive, the α -In₂Se₃ must be *n*-type, consistent with previous observations^{24,25}. Similar features in I_D *vs.* V_{DS} characteristics were seen in other samples (Fig. S2). Interestingly, a marked change in the slope was found in most I_D *vs.* V_{DS} curves, showing that I_D increases much faster at low V_{DS} than at high V_{DS} values. The sharp rise in I_D at low V_{DS} values (below a few tenth of volts) may be related to the the presence of two back-to-back Schottky diodes studied previously in other materials^{26,27}. Behavior seen at high V_{DS} values, in particular, in the linear plots (Fig. S2 and S3), is similar to what reported previously⁶.

Clockwise transfer curves of I_D *vs.* V_G , starting at $V_G = -75$ V, were measured on our FeSmFET devices at fixed temperatures, T , from 300 to 2 K (Fig. 3 and Fig. S5). These results are consistent with those seen in the previous work⁶. The clockwise hysteresis loop points to the presence of a polarization in the *n*-type α -In₂Se₃ semiconductor. Basically, at a sufficiently large negative V_G , say, -75 V, the downward pointing electric field will force the polarization inside the α -In₂Se₃ crystal downward (Figs. S1), resulting in *positive* bound surface charge on the *bottom* surface of

the crystal due to the presence of the polarization. Consequently, the energy bands will band upward (Fig. S1). The gate voltage induced *positive* charge carriers will deplete the conduction band (the existing negative charge carriers will be “drained” from the channel), which will shut down conduction channels between the source and the drain. On the *top* of the α -In₂Se₃ crystal, however, the *negative* bound charge from the downward pointing polarization will push down the conduction band, placing the Fermi energy within the conduction band (Fig. S1). However, even though the low density of the gate voltage-induced *positive* charge carriers they cannot deplete the conduction band fully because the gate electric field is weak on the top surface of the crystal, no conduction channel between the source and the drain is expected there either because of the low carrier density. An “off” state of the FeSmFET is thus expected, which was indeed observed.

As V_G increased from the -75 V to 0 and then 75 V, the polarization will start to reverse locally. The depletion layer on the bottom surface of the α -In₂Se₃ crystal will be reduced, helping push down the conduction band. A conduction channel between the source and the drain will eventually be established, leading to the “on” state of the FeSmFET. The device will continue to be in the “on” state as V_G is increased further to 75 V. Now the polarization will switch to point upward so that the bound charge from the polarization will be negative on the bottom surface of the crystal, featuring negative mobile charge carriers induced by the positive gate voltage. Ramping V_G from 75 V to 0, the polarization will turn downwards locally, leading to *positive* bound charge from the polarization on the *bottom* surface of the crystal. The existing and gate induced *negative* charge carriers could be bound to the *positive* surface charge from the polarization, creating local areas that are non-conducting. As the gate voltage decreases further, the polarization will continue to flip, leading to continued growth of non-conducting areas and a decreasing I_D . Eventually all conduction channels disappear, leading to vanishingly small I_D . A clockwise hysteresis loop as shown in Fig. 3 will be obtained. Our observation is therefore fully consistent with the existence of polarization in α -In₂Se₃, as argued previously⁶.

The overall hysteresis decreased as the temperature T was lowered (Fig. 3). Thus, it is natural to ask whether the reduction in hysteresis was a result of a change in coercive field as the temperature was lowered. This seems to be unlikely given that the ferroelectric transition temperature, T_c , of α -In₂Se₃ was reported to be 700 K¹⁹ as the coercive field of a ferroelectric material would increase as T is lowered below T_c ^{28,29} or stay as a constant far below it. The more likely scenario is the decrease in hysteresis as T was lowered was due to the presence of charge traps in our sample.

Charge traps in FETs are known to lead to a hysteresis loop. At higher temperatures, the hysteresis originating from charge traps and that from polarization appear to coexist in our samples. However, at a liquid-helium temperature, at which the binding and unbinding of mobile charge carriers from their traps are expected to be suppressed, the observed hysteresis should be only due to the reversal of the polarization, as argued previously⁶.

Values of two-point resistance R_{DS} ($= I_D/V_{DS}$, taken from the top of the hysteresis loop) are plotted against T in Fig. 4a, showing decreasing R_{DS} with the lowering T and the emergence of a metallic state. The four-point sample resistance, $R(T)$, of the same crystal was also measured as a function of T (inset of Fig. 4a), showing that $R_{DS}(T)$ and $R(T)$ have similar behavior. This suggests that the contact resistance between Ti/Au and α -In₂Se₃, which was measured at the room temperature (Fig. S7), did not make a big difference in the behavior of I_D . Data obtained for $V_G = 75$ V in samples B and C showed a positive dR/dT at higher temperatures and a complete flattening-off in $R_{DS}(T)$ down to 4 K (Figs. 4b and S6). A small negative dR/dT was seen at lowest temperatures in Sample A, even at $V_G = 75$ V where the density of gate voltage induced mobile charge carriers is the largest, appears to be due to sample specific disorder. Weak localization in a weakly disordered metallic sample can lead to a negative dR/dT when T is sufficiently low³⁰. The maximum 2D electric conductivity obtained from the four-point measurements was found to be around $80 \sigma_0$, where $\sigma_0 = e^2/h$ ($= 4.08 \times 10^{-5} \Omega^{-1}$) is the quantum conductance, e is the electron charge and h is Planck's constant. Above σ_0 , a negative dR/dT is expected due to weak localization, along with positive or negative magnetoconductance (MC) depending on the strength of the spin-orbital coupling³⁰. Our measurements showed positive MC at 1.8 K (Fig. 4c), as well as 10 K and 50 K (data not shown), consistent with the weak spin-orbital coupling expected for α -In₂Se₃. The MC data was shown in Fig. 4c to fit Maekawa-Fukuyama theory of 2D weak localization³¹ quantitatively.

In the metallic state, the negative mobile charge carriers should be accumulated near the bottom of the α -In₂Se₃ crystal while the rest of the crystal remains semiconducting. This layer of mobile charge will tend to screen the gate electric field, making the polarization in the semiconducting region of the crystal less affected by the gate electric field. However, as shown in the data, some of polarization can still be reoriented by the field even in the metallic state. As a result, the 2D metallic sheet of electrons and the polarization must coexist in α -In₂Se₃.

The interesting question is how the bound charge of polarization on the crystal bottom will affect the accumulation of the mobile electrons. At $V_G = 75$ V the electric field is expected to induce an electron density of $5 \times 10^{12}/\text{cm}^2$. Hall measurements showed that the Hall voltage is a linear function of the magnetic field, suggesting that only electrons are present in the sample. The density of electrons at 4 K is roughly what would be expected solely from that induced by the gate electric field, unaffected by the polarization (Fig. 4d). At higher temperatures however, the electron density obtained by the Hall measurements is larger than that induced by the gate voltage. This is reasonable, as the existing unintentionally doped electrons that are bound to the positive charge traps at low temperatures would start to be released as the temperature was raised, consistent with the observation of the broadening hysteresis noted above.

The observations presented above demonstrate a well-functioning FET with a large I_D even when gate voltage is at zero. Such a FeSmFET can be used for logic operations as well as a memory device in the microelectronic circuitry with the “logic in memory” functionalities. In addition, ultrathin $\alpha\text{-In}_2\text{Se}_3$ was shown to provide a testbed for fundamental research on ferroelectric metals as well as ferroelectric metal-insulator transitions tuned by a gate voltage.

Acknowledgement. Work is supported by the NSF (Grant No. EFMA1433378). The $\alpha\text{-In}_2\text{Se}_3$ crystals used in this study were produced by the Penn State 2D Crystal Consortium – Materials Innovation Platform (2DCC-MIP) under NSF cooperative agreement DMR-1539916.

Data Availability. The data that support the findings of this study are available from the corresponding author upon reasonable request.

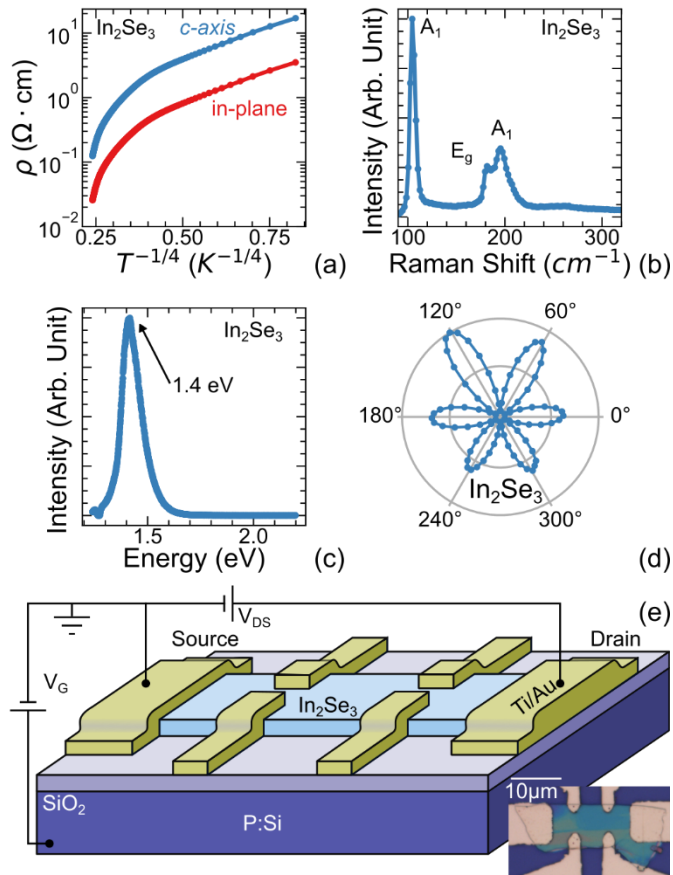


Fig. 1. (a) In- and out-of-plane resistivities of bulk single-crystals α - In_2Se_3 showing Mott variable-range hopping conduction behavior, $\rho_{\text{in-plane, c-axis}}(T) \sim \exp[(T_0/T)^{1/4}]$, where T_0 is a constant, below around $T = 160$ K. Also shown are results of Raman spectroscopy (b), photoluminescence (c), and second harmonic generation (d) measurements. A schematic of an FeSmFET in the Hall bar pattern is shown in (e). Inset: Optical image of a FeSmFET device following this design with the 10- μm scale bar also shown.

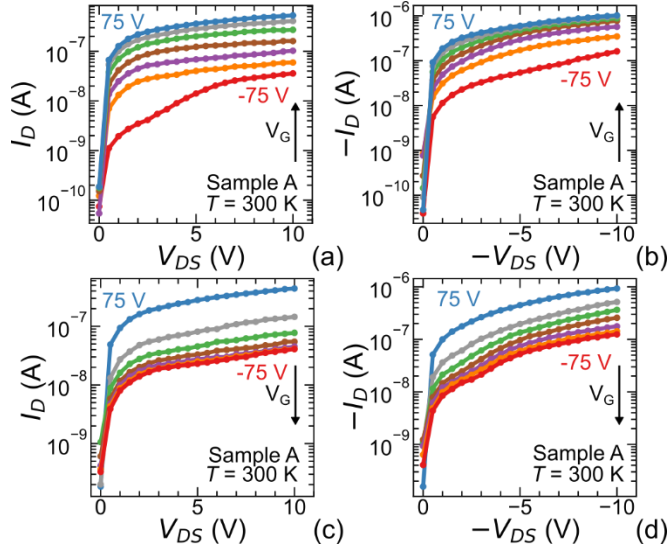


Fig. 2. Curves of I_D - V_{DS} for Sample A obtained at room temperature for fixed gate voltages in an increasing order, $V_G = -75, -50, -25, 0, 25, 50, 75$ V at a positive (a) and negative (b) values of V_{DS} . Corresponding I_D - V_{DS} curves for decreasing V_G at the same gate voltages are shown in (c) and (d).

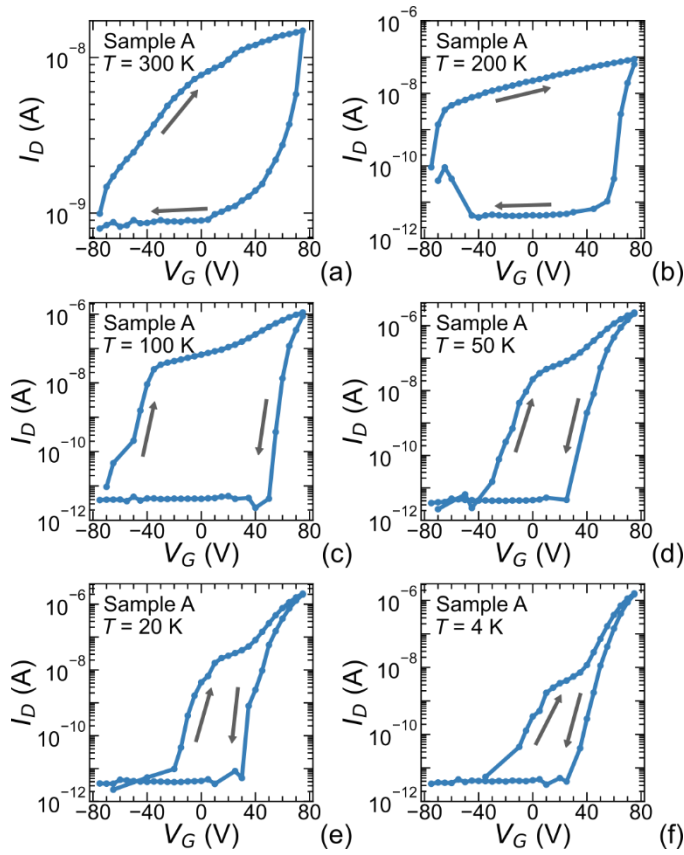


Fig. 3. (a-f) Transfer curves of source-drain current vs. gate voltage, I_D vs. V_G , obtained at fixed temperatures (T) as indicated. V_G was initially decreased from 0 to -75 V, after which V_G was

ramped from -75 to 75 V and then back to -75 V while the I_D vs. V_G curve was measured. A clockwise hysteresis loop was obtained at each temperature.

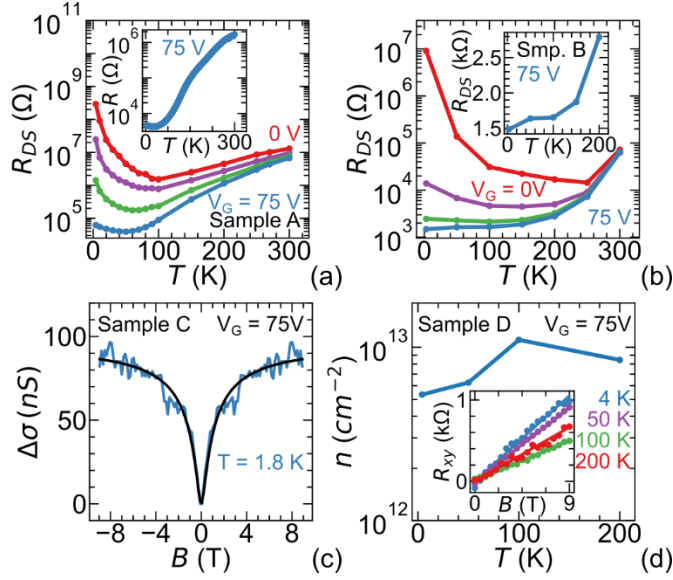


Fig. 4. (a) Two-point sample resistance, $R_{SD}(T)$ ($R_{DS} = I_D/V_{DS}$) obtained at $V_G = 0, 25, 50,$ and 75 V, in the top portion of the clockwise hysteresis loops taken at fixed temperatures for Sample A. Inset: Four-point resistance vs. temperature, $R(T)$, measured while the device was warming up after it was cooled to 4 K at $V_G = -75$ V followed by ramping V_G from -75 to 75 V at 4 K. (b) $R_{DS}(T)$ for Sample B in semi-log plot obtained from the top portion of clockwise hysteresis loops. Inset: $R_{DS}(T)$ for $V_G = 75$ V in linear plot. (c) Magnetoconductance at $T = 1.8$ K and $V_G = 75$ V for Sample C. The Maekawa-Fukuyama theory was shown to fit the data (see main text). (d) Charge carrier density, n , as a function of T for Sample D. The device design for Samples A and D is shown in Fig. 1e and that for Samples B and C is shown in Fig. S1 (a).

Supplementary Materials

Table S1. Parameters for 4 devices studied in the current work, where t is the thickness of the α - In_2Se_3 crystal, L is the channel length (length between the voltage leads), w is the channel width, and ΔV_G is the size of the hysteresis loop measured at $I_D = 1 \text{ nA}$ and $T = 300 \text{ K}$.

Sample	t (nm)	L (μm)	w (μm)	Device pattern	ΔV_G (V) at 1nA and 300K
A	110	14	10	Hall bar	87V
B	13	5	30	Standard FET	19V
C	20	2	5	Standard FET	23V
D	110	14	9	Hall bar	not measured

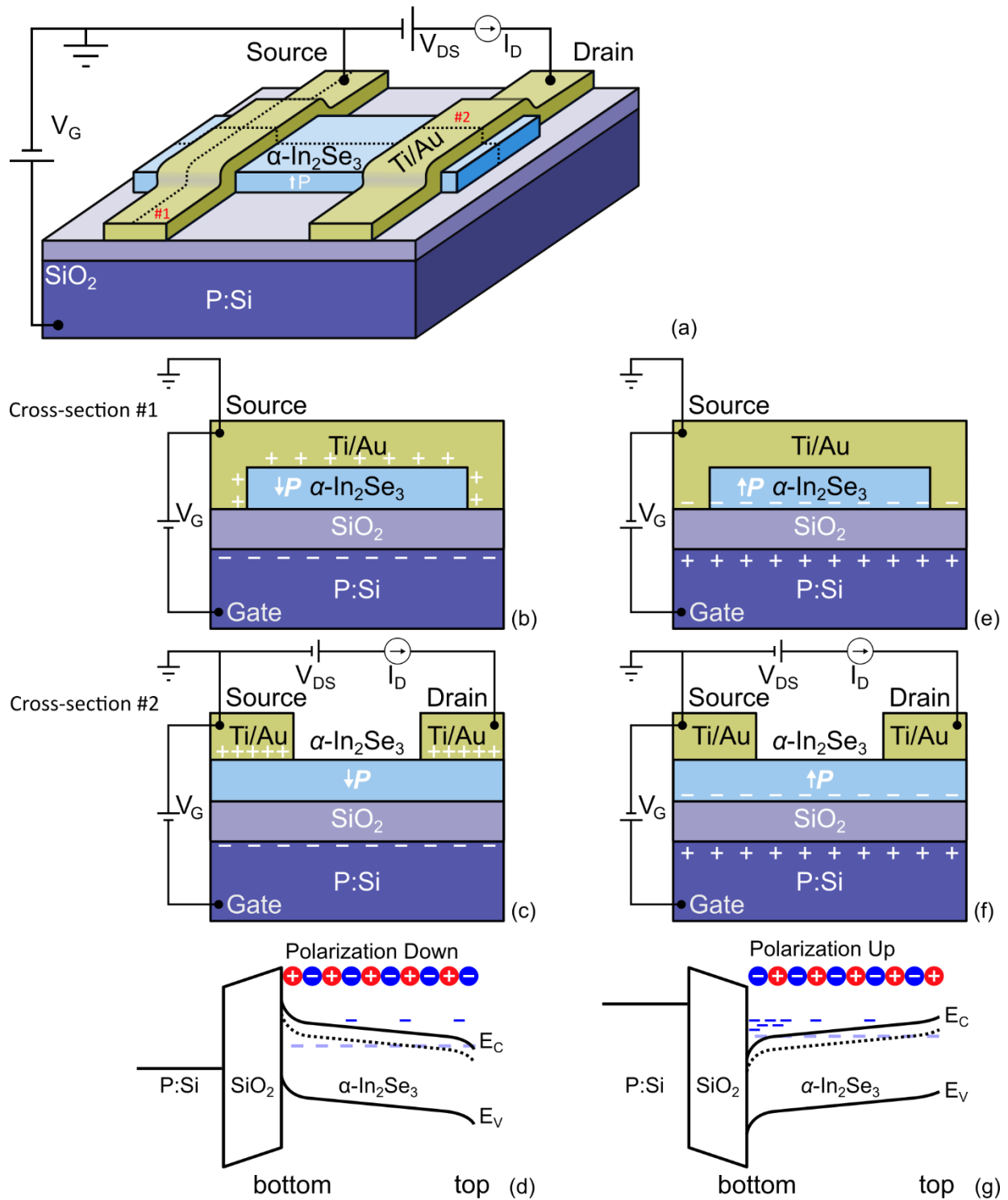


Fig. S1. a) Schematic of FeSmFET adopted in Samples B and C. b-c) Cross sectional views of the device cut along the dashed lines marked by #1 and #2 in a), perpendicular to and along the direction of I_D , respectively, for $V_{SD} = 0.1$ V and $V_{SD} = -75$. The polarization is pointing downwards.

d) Band diagrams along the vertical direction in (c) near the center of the α -In₂Se₃ channel is shown for $V_{SD} = -75$ V. The mobile charge carriers are marked by +/- signs while the bound charge from electrical polarization is marked by the +/- circles. The crystal of α -In₂Se₃ is unintentionally doped and n -type with the impurity states formed slightly below the bottom of the conduction band (black dashed line). The band bending on the top and bottom surfaces of the α -In₂Se₃ crystal is assumed to be induced by only the bound surface charge from the polarization. The location of the Fermi level (dashed blue line) is determined by the existing charge carriers. The bottom layer of the crystal is depleted at $V_{SD} = -75$ V. e-f) Cross sectional views of the device cut along the dashed lines marked by #1 and #2 in a), respectively for $V_{SD} = 0.1$ V and $V_{SD} = 75$. The polarization is pointing upwards. g) The band along the vertical direction in (f) near the center of the α -In₂Se₃ channel is shown for $V_{SD} = 75$ V. The location of the Fermi level is indicated by blue dashed line. The impurity states are formed slightly below the bottom of the conduction band (black dashed line). The accumulation of mobile electrons near the bottom surface of the crystal, the tilting of the energy band due to the existing of a finite electric field, and the existence of electrons from the impurity states in the interior of the α -In₂Se₃ crystal are shown schematically, when appropriate.

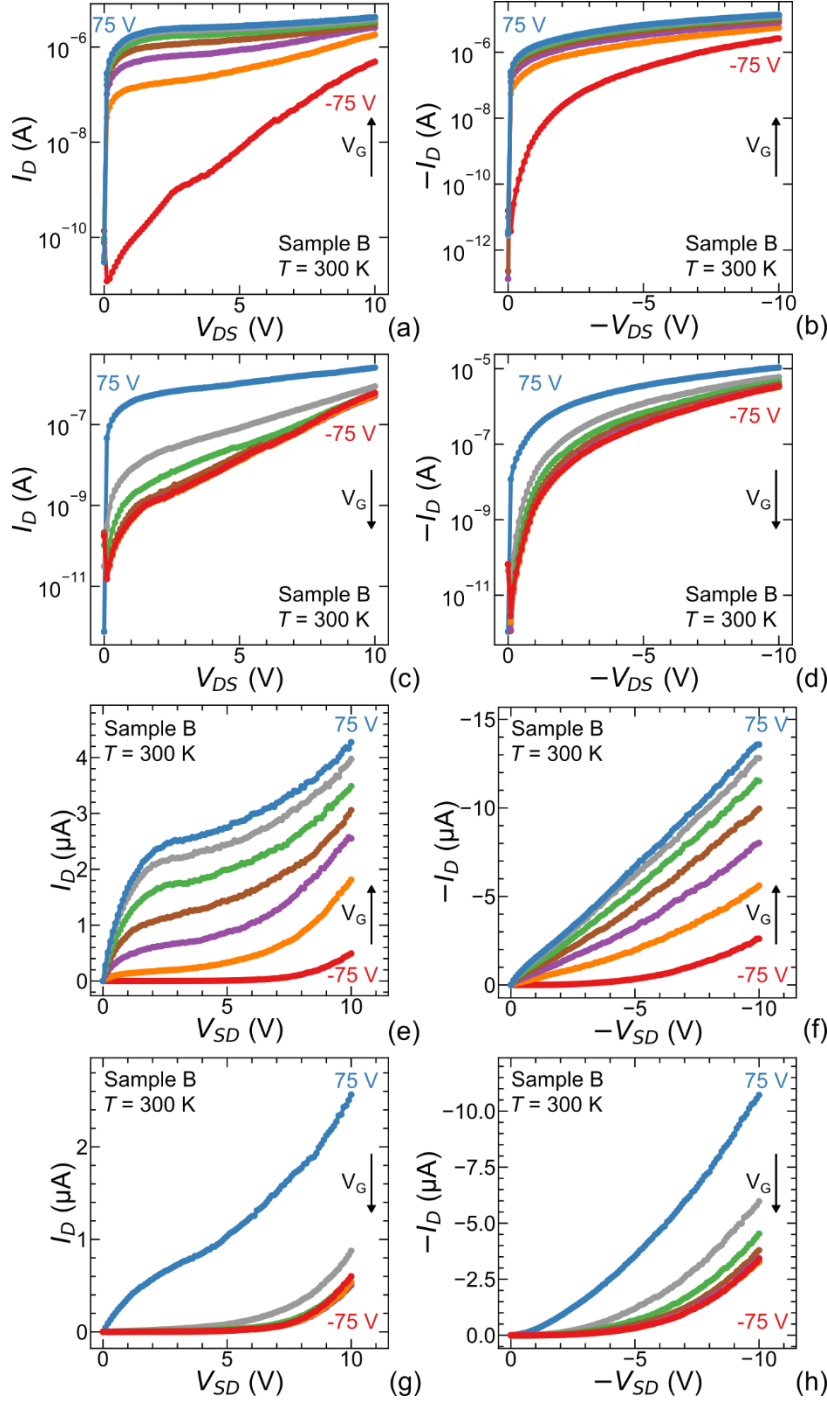


Fig. S2. I_D vs. V_{DS} measured in Sample B. V_G was fixed for each curve in 25 V increments from -75 V to 75 V, the same as that shown in Fig. 2 in the main text, for positive (a) and negative (b) V_{DS} . c-d). Corresponding positive and negative I_D vs. V_{DS} while V_G is decreased from 75 V to -75 V in 25 V increments. All measurements were done at 300 K. The linear plots of the same data are shown in e-h).

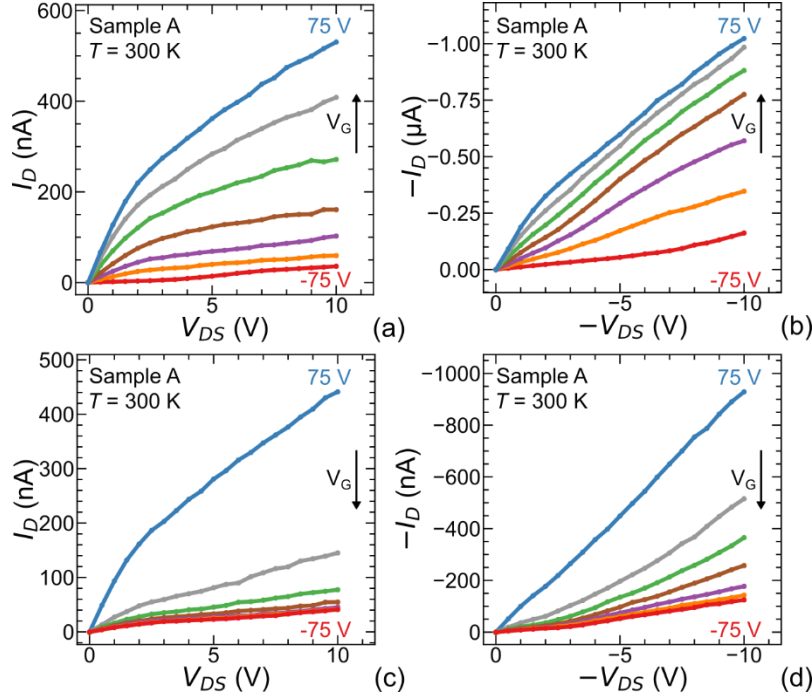


Fig. S3. I_D vs. V_{DS} data obtained in Sample A (shown in Fig. 2 of the main text in a semilog plot) plotted in the linear scale. Gate voltages V_G was in an increasing order, $V_G = -75, -50, -25, 0, 25, 50, 75$ V at a positive (a) and negative (b) values of V_{DS} . Corresponding I_D - V_{DS} curves for decreasing V_G at the same gate voltages are shown in (c) and (d). All measurements were done at 300 K.

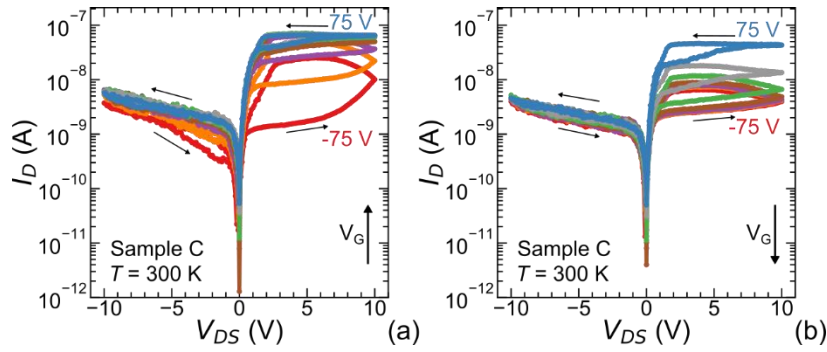


Fig. S4. I_D vs. V_{DS} measured in Sample C with increasing and decreasing gate voltage measured at $T = 300$ K. The sign of the I_D reversed for negative V_{DS} to facilitate the semi-log plotting. Gate voltage V_G was increased in (a) and decreased in (b) in 25 V increments from -75 V to 75 V. After V_G was set, the V_{DS} was increased then decreased from 0 to -10V and back (not shown for clarity), then from 0 V, to 10 V, to -10 V and finally to 0 V. Note that the maximum current is smaller than shown in Fig. S6 below as the data was taken after the sample was left at room temperature for an extended time, resulting in a small degradation of the sample from previous measurements.

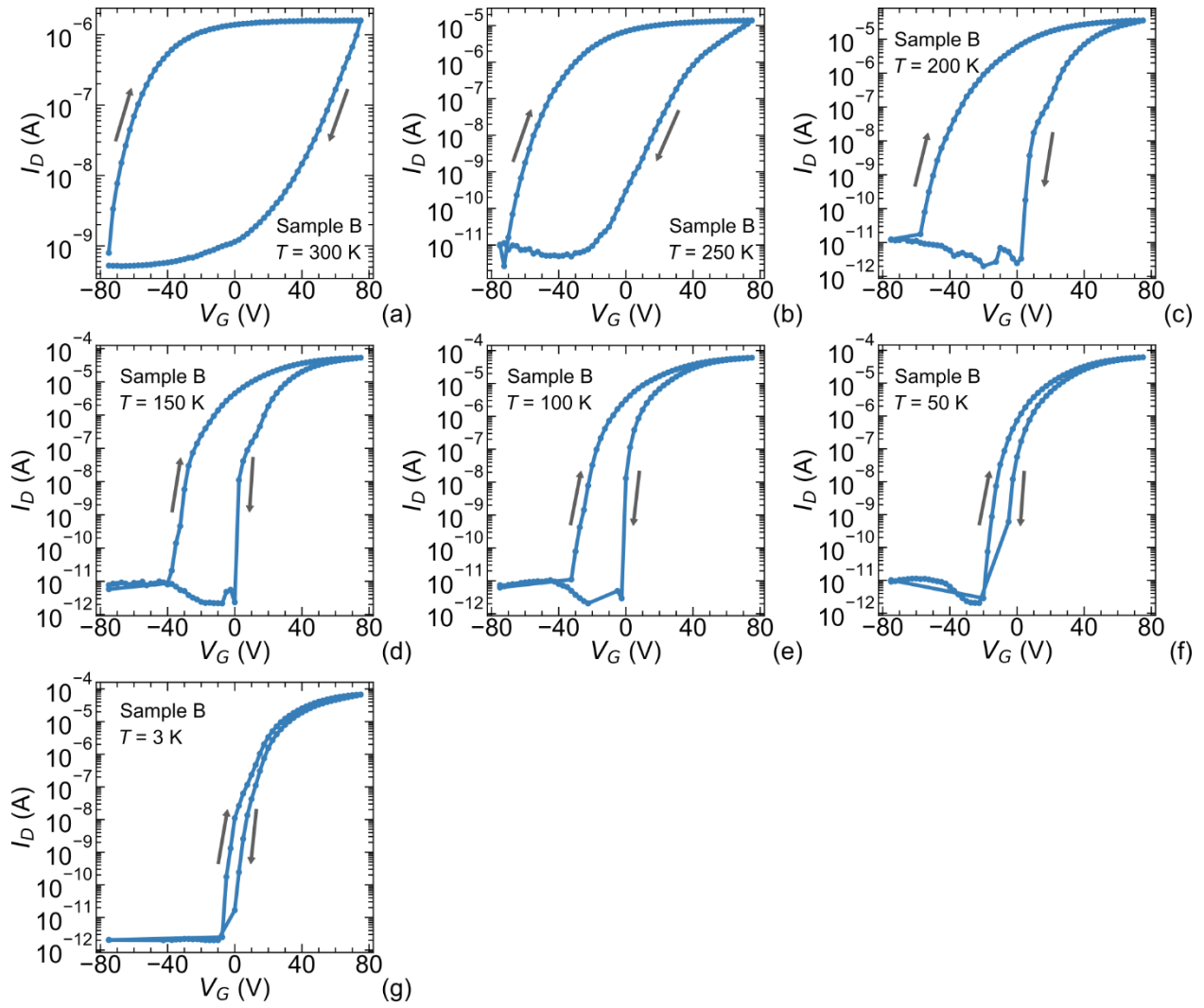


Fig. S5. a-g) The transfer curves of I_D vs. V_G of Sample B, performed using the same procedure as Sample A (shown in Fig. 3 in the main text). $V_{DS} = 0.1$ V for all measurements. $V_G = 25$ V, 50 V, and 75 V for upper portion of loop is used for Fig. 4b in the main text.

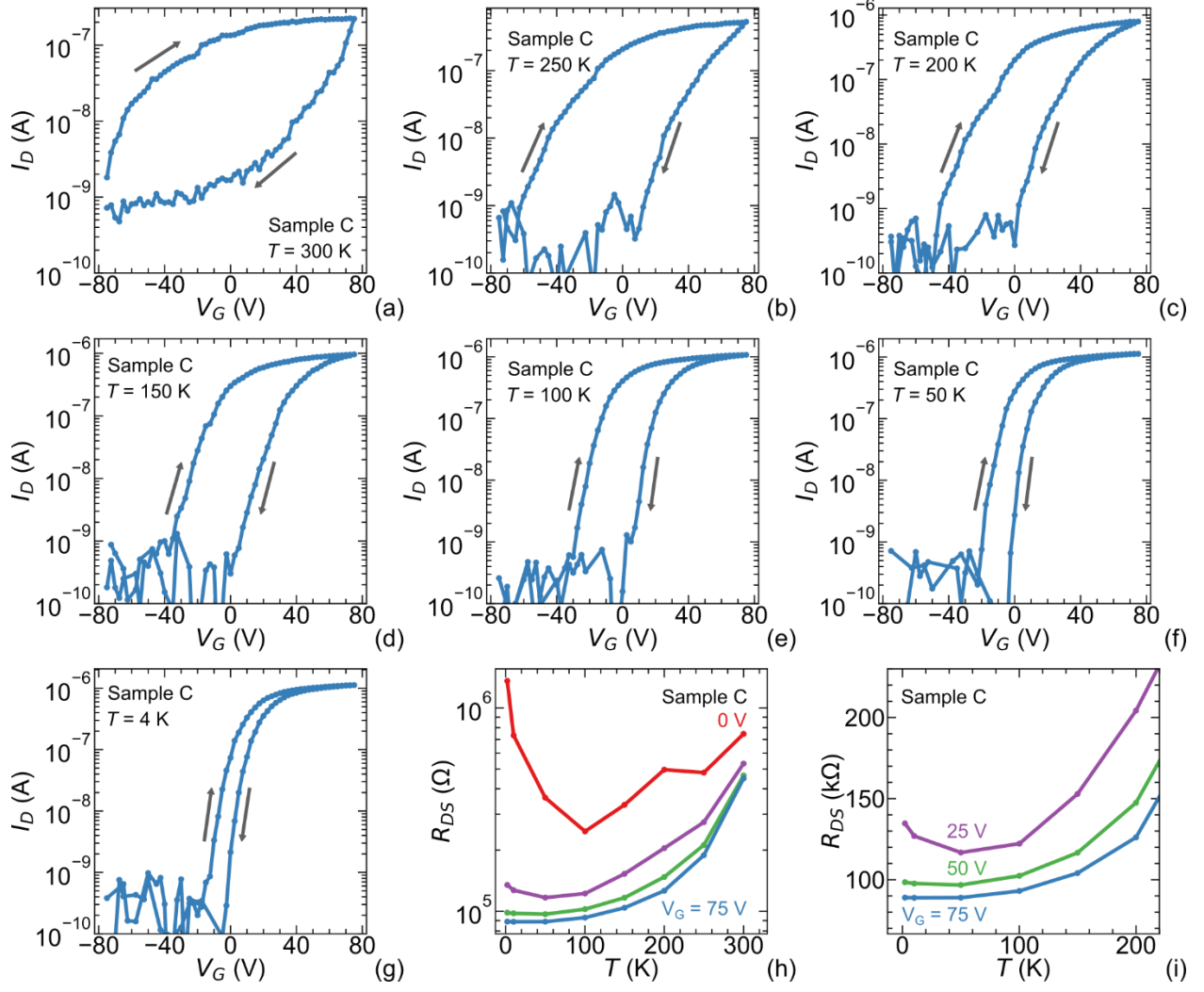


Fig. S6. a-g) The transfer curves of I_D vs. V_G of Sample C performed using the same procedure as Sample A shown in Fig. 3 in the main text; $V_{DS} = 0.1$ V for all measurements. h). $R_{DS}(T, V_G)$ taken from the clockwise hysteresis loops of I_D vs. V_G curves a-g, showing the same behavior seen in Figs. 4a-b in the main text. i) Low-temperature data from (h) shown in a linear plot for comparison.

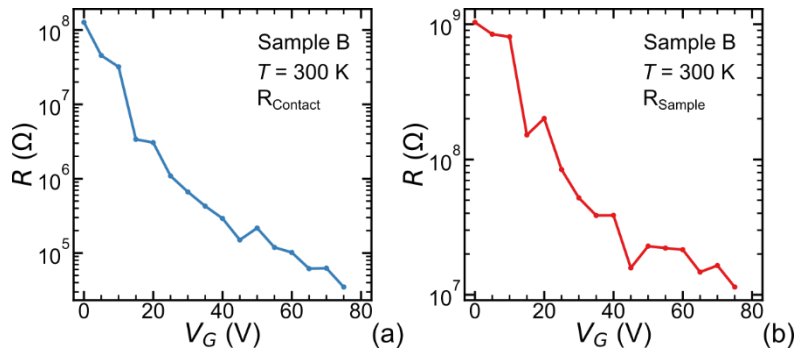


Fig. S7. a) Contact resistance between α - In_2Se_3 and Ti/Au leads measured with a $V_{\text{DS}} = 0.1$ V bias between source and drain leads using a 3-point lead configuration at room temperature. b) 4-point resistance of the sample.

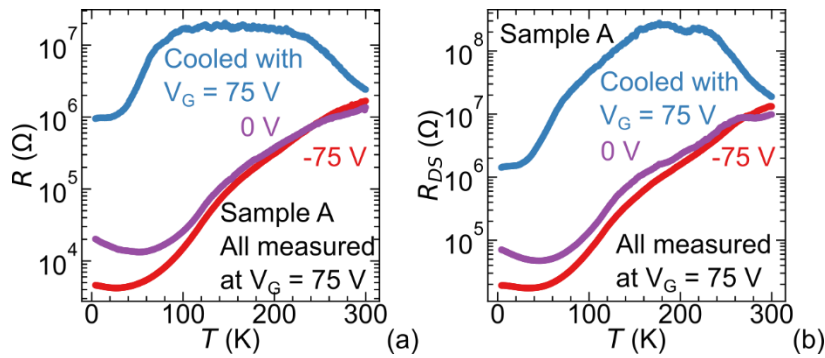


Fig. S8. History dependence of $R(T)$ and $R_{\text{DS}}(T)$ of Sample A. V_G was ramped from 0 to -75 V at 300 K, then cooled to 4K with V_G ramped to and fixed at -75 V, 0 V, or 75V. At $T = 4$ K, V_G was ramped again going through the full hysteresis loop clockwise to $V_G = 75$ V before R was measured as a function of increasing T while V_G is fixed at that value. R is seen to be the smallest when the sample was cooled at $V_G = -75$ V.

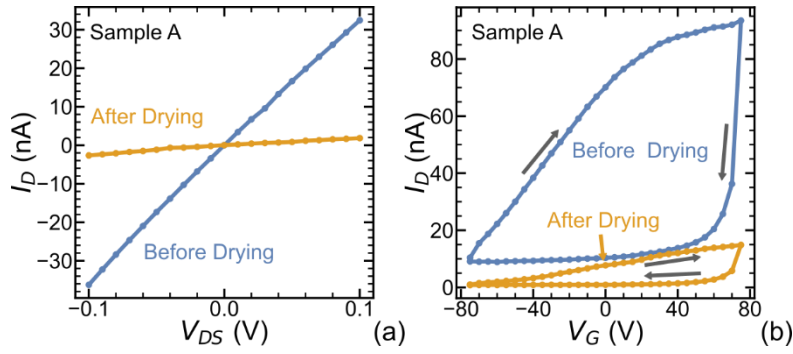


Fig. S9. Detection of charge traps at the interface between α - In_2Se_3 and SiO_2 . a) I_D - V_{DS} , curves for Sample A before and after the “drying” - The sample was “dried” by heating to 400 K in high vacuum for one hour within the PPMS was kept at 400 K for an hour to remove water molecules trapped at the interface. b) The transfer curves of source-drain current *vs.* gate voltage, I_D *vs.* V_G , at 300 K before and after the “drying”. The measurements were taken immediately before and after “drying”.

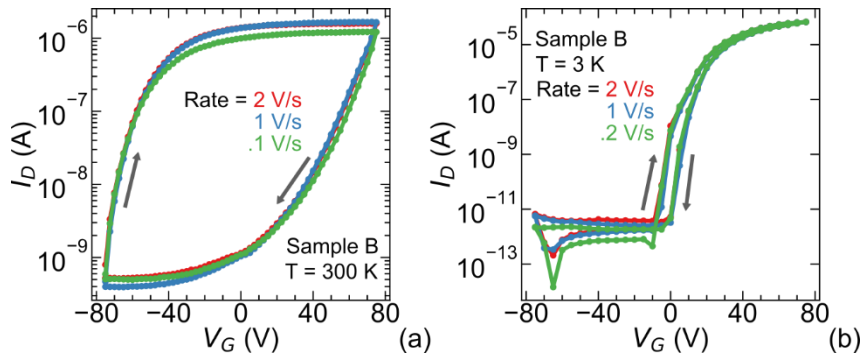


Fig. S10. Rate dependence on hysteresis loops of Sample B. Transfer curves of I_D *vs.* V_G take at different sweeping rates at 300 K (a) and 3 K (b).

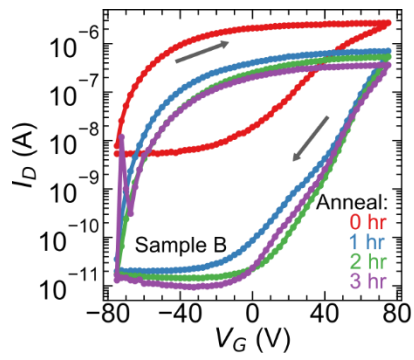


Fig. S11. Transfer curves of source-drain current vs. gate voltage, I_D vs. V_G , at 300 K before and after the sample was dried by heating to 400 K in a high vacuum for one hour in the PPMS then cooled down to room temperature to be remeasured. This was repeated two additional times for a total of 3 hours of heating at 400 K.

References

- ¹ G. A. Smolenskii, V. A. Bokov, V. A. Isupov, N. N. Krainik, R. E. Pasinkov, and I. A. Sokolov. *Ferroelectrics and Related Materials* Gordon and Breach Science Publishers (1984).
- ² S. Dünkel, M. Trentzsch, R. Richter, P. Moll, C. Fuchs, O. Gehring, M. Majer, S. Wittek, B. Müller, T. Melde, H. Mulaosmanovic, S. Slesazeck, S. Müller, J. Ocker, M. Noack, D.-A. Löhr, P. Polakowski, J. Müller, T. Mikolajick, J. Höntschel, B. Rice, J. Pellerin, and S. Beyer. A FeFET based super-low-power ultra-fast embedded NVM technology for 22nm FDSOI and beyond, in *2017 IEEE International Electron Devices Meeting (IEDM)*, pp. 19.7.1-19.7.4. <https://doi.org/10.1109/iedm.2017.8268425>.
- ³ Mengwei Si, Pai-Ying Liao, Gang Qiu, Yuqin Duan, and Peide D. Ye. Ferroelectric Field-Effect Transistors Based on MoS₂ and CuInP₂S₆ Two-Dimensional van der Waals Heterostructure. *ACS Nano* 2018 **12**(7), 6700–6705 (2018). <https://doi.org/10.1021/acsnano.8b01810>.
- ⁴ T.P. Ma and Jin-Ping Han. Why is nonvolatile ferroelectric memory field-effect transistor still elusive? *IEEE Electron Device Letters* 2002 **23**(7), 386–388 (2002). <https://doi.org/10.1109/LED.2002.1015207>.
- ⁵ Wenwu Xiao, Chen Liu, Yue Peng, Shuaizhi Zheng, Qian Feng, Chunfu Zhang, Jincheng Zhang, Yue Hao, Min Liao and Yichun Zhou, “Memory Window and Endurance Improvement of Hf_{0.5}Zr_{0.5}O₂-Based FeFETs with ZrO₂ Seed Layers Characterized by Fast Voltage Pulse Measurements. *Nanoscale Research Letters* 14, 254 (2019). <https://doi.org/10.1186/s11671-019-3063-2>.
- ⁶ Mengwei Si, Atanu K. Saha, Shengjie Gao, Gang Qiu, Jingkai Qin, Yuqin Duan, Jie Jian, Chang Niu, Haiyan Wang, Wenzhuo Wu, Sumeet K. Gupta, and Peide D. Ye. A ferroelectric semiconductor field-effect transistor. *Nat Electron* 2019 1–7 (2019). <https://doi.org/10.1038/s41928-019-0338-7>.

⁷ P. W. Anderson and E. I. Blount. Symmetry Considerations on Martensitic Transformations: “Ferroelectric” Metals? *Phys. Rev. Lett.* 1965 **14**(7), 217–219 (1965).

<https://doi.org/10.1103/physrevlett.14.217>.

⁸ Youguo Shi, Yanfeng Guo, Xia Wang, Andrew J. Princep, Dmitry Khalyavin, Pascal Manuel, Yuichi Michiue, Akira Sato, Kenji Tsuda, Shan Yu, Masao Arai, Yuichi Shirako, Masaki Akaogi, Nanlin Wang, Kazunari Yamaura, and Andrew T. Boothroyd. A ferroelectric-like structural transition in a metal. *Nature Mater* 2013 **12**(11), 1024–1027 (2013).

<https://doi.org/10.1038/nmat3754>.

⁹ Nicole A. Benedek and Turan Birol. “Ferroelectric” metals reexamined: fundamental mechanisms and design considerations for new materials. *J. Mater. Chem. C* 2016 **4**(18), 4000–4015 (2016). <https://doi.org/10.1039/c5tc03856a>.

¹⁰ Shiming Lei, Mingqiang Gu, Danilo Puggioni, Greg Stone, Jin Peng, Jianjian Ge, Yu Wang, Baoming Wang, Yakun Yuan, Ke Wang, Zhiqiang Mao, James M. Rondinelli, and Venkatraman Gopalan. Observation of Quasi-Two-Dimensional Polar Domains and Ferroelastic Switching in a Metal, $\text{Ca}_3\text{Ru}_2\text{O}_7$. *Nano Lett.* 2018 **18**(5), 3088–3095 (2018).

<https://doi.org/10.1021/acs.nanolett.8b00633>.

¹¹ T. H. Kim, D. Puggioni, Y. Yuan, L. Xie, H. Zhou, N. Campbell, P. J. Ryan, Y. Choi, J.-W. Kim, J. R. Patzner, S. Ryu, J. P. Podkaminer, J. Irwin, Y. Ma, C. J. Fennie, M. S. Rzchowski, X. Q. Pan, V. Gopalan, J. M. Rondinelli, and C. B. Eom. Polar metals by geometric design. *Nature* 2016 **533**(7601), 68–72 (2016). <https://doi.org/10.1038/nature17628>.

¹² Zaiyao Fei, Wenjin Zhao, Tauno A. Palomaki, Bosong Sun, Moira K. Miller, Zhiying Zhao, Jiaqiang Yan, Xiaodong Xu, and David H. Cobden. Ferroelectric switching of a two-dimensional metal. *Nature* 2018 **560**(7718), 336–339 (2018). <https://doi.org/10.1038/s41586-018-0336-3>.

¹³ Wenjun Ding, Jianbao Zhu, Zhe Wang, Yanfei Gao, Di Xiao, Yi Gu, Zhenyu Zhang, and Wenguang Zhu. Prediction of intrinsic two-dimensional ferroelectrics in In_2Se_3 and other III_2 -

VI₃ van der Waals materials. *Nat Commun* 2017 **8**(1), 1–8 (2017).

<https://doi.org/10.1038/ncomms14956>.

¹⁴ Chaojie Cui, Wei-Jin Hu, Xingxu Yan, Christopher Addiego, Wenpei Gao, Yao Wang, Zhe Wang, Linze Li, Yingchun Cheng, Peng Li, Xixiang Zhang, Husam N. Alshareef, Tom Wu, Wenguang Zhu, Xiaoqing Pan, and Lain-Jong Li. Intercorrelated In-Plane and Out-of-Plane Ferroelectricity in Ultrathin Two-Dimensional Layered Semiconductor In₂Se₃. *Nano Lett.* 2018 **18**(2), 1253–1258 (2018). <https://doi.org/10.1021/acs.nanolett.7b04852>.

¹⁵ Siyuan Wan, Yue Li, Wei Li, Xiaoyu Mao, Wenguang Zhu, and Hualing Zeng. Room-temperature ferroelectricity and a switchable diode effect in two-dimensional α -In₂Se₃ thin layers. *Nanoscale* 2018 **10**(31), 14885–14892 (2018). <https://doi.org/10.1039/C8NR04422H>.

¹⁶ Pengfei Hou, Yang Lv, Xiangli Zhong, and Jinbin Wang. α -In₂Se₃ Nanoflakes Modulated by Ferroelectric Polarization and Pt Nanodots for Photodetection. *ACS Appl. Nano Mater.* 2019 **2**(7), 4443–4450 (2019). <https://doi.org/10.1039/c9ra06566k>.

¹⁷ Pengfei Hou, Siwei Xing, Xin Liu, Cheng Chen, Xiangli Zhong, Jinbin Wang, and Xiaoping Ouyang. Resistive switching behavior in α -In₂Se₃ nanoflakes modulated by ferroelectric polarization and interface defects. *RSC Advances* 2019 **9**(52), 30565–30569 (2019). <https://doi.org/10/ggpp3s>.

¹⁸ Mingjin Dai, Kai Li, Fakun Wang, Yunxia Hu, Jia Zhang, Tianyou Zhai, Bin Yang, Yongqing Fu, Wenwu Cao, Dechang Jia, Yu Zhou, and PingAn Hu. Intrinsic Dipole Coupling in 2D van der Waals Ferroelectrics for Gate-Controlled Switchable Rectifier. *Advanced Electronic Materials* 2020 **6**(2), 1900975 (2020). <https://doi.org/10.1002/aelm.201900975>.

¹⁹ Jun Xiao, Hanyu Zhu, Ying Wang, Wei Feng, Yunxia Hu, Arvind Dasgupta, Yimo Han, Yuan Wang, David A. Muller, Lane W. Martin, PingAn Hu, and Xiang Zhang. Intrinsic Two-Dimensional Ferroelectricity with Dipole Locking. *Phys. Rev. Lett.* 2018 **120**(22), 227601 (2018). <https://doi.org/10.1103/physrevlett.120.227601>.

-
- ²⁰ Yu Zhou, Di Wu, Yihan Zhu, Yujin Cho, Qing He, Xiao Yang, Kevin Herrera, Zhaodong Chu, Yu Han, Michael C. Downer, Hailin Peng, and Keji Lai. Out-of-Plane Piezoelectricity and Ferroelectricity in Layered α -In₂Se₃ Nanoflakes. *Nano Lett.* 2017 **17**(9), 5508–5513 (2017). <https://doi.org/10.1021/acs.nanolett.7b02198>.
- ²¹ Huai Yang, Mengqi Xiao, Yu Cui, Longfei Pan, Kai Zhao, and Zhongming Wei. Nonvolatile memristor based on heterostructure of 2D room-temperature ferroelectric α -In₂Se₃ and WSe₂. *Sci. China Inf. Sci.* 2019 **62**(12), 1–8 (2019). <https://doi.org/10.1007/s11432-019-1474-3>.
- ²² Siyuan Wan, Yue Li, Wei Li, Xiaoyu Mao, Chen Wang, Chen Chen, Jiyu Dong, Anmin Nie, Jianyong Xiang, Zhongyuan Liu, Wenguang Zhu, and Hualing Zeng. Nonvolatile Ferroelectric Memory Effect in Ultrathin α -In₂Se₃. *Advanced Functional Materials* 2019 **29**(20), 1808606 (2019). <https://doi.org/10.1002/adfm.201808606>.
- ²³ Nilanthy Balakrishnan, Elisabeth D. Steer, Emily F. Smith, Zakhar R. Kudrynskiy, Zakhar D. Kovalyuk, Laurence Eaves, Amalia Patanè, and Peter H. Beton. Epitaxial growth of γ -InSe and α , β , and γ -In₂Se₃ on ϵ -GaSe. *2D Mater.* 2018 **5**(3), 035026 (2018). <https://doi.org/10.1088/2053-1583/aac479>.
- ²⁴ C. Julien, M. Eddrief, K. Kambas, and M. Balkanski. Electrical and optical properties of In₂Se₃ thin films. *Thin Solid Films* 1986 **137**(1), 27–37 (1986). [https://doi.org/10.1016/0040-6090\(86\)90191-4](https://doi.org/10.1016/0040-6090(86)90191-4).
- ²⁵ J. O. Island, S. I. Blanter, M. Buscema, H. S. J. van der Zant, and A. Castellanos-Gomez. Gate Controlled Photocurrent Generation Mechanisms in High-Gain In₂Se₃ Phototransistors. *Nano Lett.* 2015 **15**(12), 7853–7858 (2015). <https://doi.org/10.1021/acs.nanolett.5b02523>.
- ²⁶ Raymond T. Tung. The physics and chemistry of the Schottky barrier height. *Applied Physics Reviews* 2014 **1**(1), 011304 (2014). <https://doi.org/10.1063/1.4858400>.

²⁷ Jozef Osvald. Back-to-back connected asymmetric Schottky diodes with series resistance as a single diode. *Phys. Status Solidi A*, **212**, 2754-2758 (2015).

<https://doi.org/10.1002/pssa.201532374>.

²⁸ Zheng Wang, Hanbin Ying, Winston Chern, Shimeng Yu, Martin Mourigal, John D. Cressler, Asif I. Khan. Cryogenic characterization of a ferroelectric field-effect-transistor. *Appl. Phys. Lett.* 2020 **116**(4), 042902 (2020). <https://doi.org/10.1063/1.5129692>.

²⁹ Yang Zhang, Zhaojiang Chen, Wenwu Cao, Zhongwu Zhang. Temperature and frequency dependence of the coercive field of 0.71PbMn_{1/3}Nb_{2/3}O₃-0.29PbTiO₃ relaxor-based ferroelectric single crystal. *Appl. Phys. Lett.* 2017 **111**(17), 172902 (2017). <https://doi.org/10.1063/1.4998187>.

³⁰ P. A. Lee and T. V. Ramakrishnan. Disordered electronic systems. *Rev. Mod. Phys.* **57**, 287 (1985). <https://doi.org/10.1103/RevModPhys.57.287>.

³¹ Sadamichi Maekawa and Hidetoshi Fukuyama. Magnetoresistance in Two-Dimensional Disordered Systems: Effects of Zeeman Splitting and Spin-Orbit Scattering. *J. Phys. Soc. Jpn.* 1981 **50**(8), 2516–2524 (1981). <https://doi.org/10.1143/jpsj.50.2516>.